Impacts of Scene Geometry and Vehicle Speed on the Performance of RFID based AVI/ETC System

Kai She
School of Physics and Electronic Science
Hunan University of Science and Technology
Xiangtan, China
shekai@126.com

Yichuang Sun
Department of Engineering and Technology
University of Hertfordshire
Hatfield, Hertfordshire, United Kingdom
y.sun@herts.ac.uk

***Abstract*—Passive UHF Radio Frequency Identification (RFID) is a potential technology for Automatic Vehicle Identification (AVI) and Electronic Toll Collection (ETC) systems. However, the identification performance is often seriously influenced by the RF radiation zone and anti-collision protocol simultaneously. The impacts of scene geometry and vehicle speed on the identification rate are analyzed and modeled for a typical AVI/ETC application scenario. A calculation method of identification zone is firstly proposed based on the ray-tracing theory. Then the communication procedure is divided into three processes, which are also modeled using individual probability methods. Numerical simulations show that there are strong influences on the tag identification rate caused by the tag speed and antenna inclination angles, and we can obtain a higher identification rate through optimizing them.**

***Index Terms*—Radio Frequency Identification (RFID), Tag Speed, Radiation Zone, Identification Rate (IR), Automatic Vehicle Identification (AVI), Electronic Toll Collection (ETC).**

I. Introduction

Passive UHF Radio Frequency Identification (RFID) technology can be used in Automatic Vehicle Identification (AVI) and Electronic Toll Collection (ETC) system for its advantages, such as wireless power supply and cheap tags [1], [2]. The identification rate (IR) is a key performance index. A successful identification mainly relies on whether the power received by the tag can activate the tag chip. Many factors will affect the process, including the antenna gain, the transmitted power, the tag chip activation threshold, and so on [3]. But among them, the reader RF radiation zone and vehicle movement would be the most unmanageable in deployment, because the others are all determined by the factory.

Researchers firstly studied the impact of RF multipath propagation based on different models. The Friss model, two-ray model, and ray-tracing model were used to estimate the real RF radiation zone of a classroom [4]. A complete link budget model for UHF RFID systems considering the gains of transmitting and receiving antennas and multipath propagation was proposed [3]. Then researchers tried to control the radiation zone through array antennas. An array antenna was manufactured to widen the readable zone [5]. Also, a kind of phase-controlled array antenna was studied to control the radiation zone and was used to avoid interferences with other lanes for ETC system [6].

On the other hand, other researchers paid extra attention to the impacts of vehicle movements and the procedure of communication determined by the anti-collision protocol. The character of nonstationary and Doppler frequency was simulated and measured for a vehicle to infrastructure scene considering the vehicle movement speed [7]. The influences of tag speed in multi-tag cases were studied simultaneously, but only a simple Poisson distribution was used to model the complex dynamical procedure [8]. Based on OMNeT++ and PyONS discrete-event simulators, the impact of parameters of protocol and propagation channels was analysed and simulated, but only statistical channel models were used in the simulation [9].

The maximum IR is influenced by the physical and data link layer simultaneously. However, nearly all the papers focus on the static RF radiation zone, and few of them can directly relate it with scene geometry and the vehicle speed simultaneously. So this paper will consider the impacts of both of them. The results will aid in the identification of the optimal geometry locations of the infrastructure to minimize power consumption and increase service performance, improving vehicular communications in AVI/ETC.

The paper is organized as follows. Section II will present a calculation method to show the impact of the scene geometry on the radiation zone for a typical RFID AVI/ETC scenario. Section III will focus on the influences of vehicle speed and the whole communication procedure using suitable probability models. Experimental results will be shown in Section IV. Finally, the conclusion is given in Section V.

II. Impact of the Scene Geometry to the Identification Zone

A. Scene Geometry

Fig. 1 shows a geometric diagram of a typical RFID based AVI/ETC system. The reader antenna is arranged above the lanes, its height is H_{reader}, its inclination angle is α. In this paper, the position of the reader antenna is set as Cartesian coordinate origin. We suppose tags are attached to the vehicle windscreen. The vehicle moves across the radiation zone in the direction of $-y$. For a car, the main reflectors are the car

The paper is sponsored by the Natural Science Foundation of Hunan Province (No.2018JJ2127)

hood, with its height H_{car}, and the bus body. Although there are other multiple reflections, they contribute much lower to the power received by the tag, which was confirmed by actual measurements of ETC toll gates [10]. Therefore, the paper will use a three-ray model to study the radiation zone based on the geometrical optics method for a typical AVI/ETC toll gate. And we believe that the prediction method of radiation zone is representative.

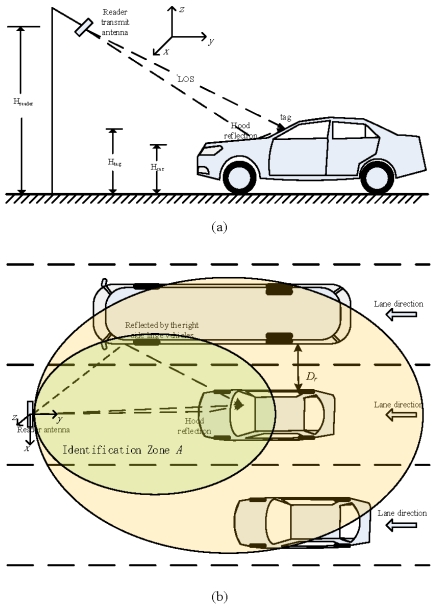

Fig. 1. The geometry of a typical AVI/ETC scenario. (a) Side view (b) Top view

B. Tag Received Power

The received power of tag comes from the power transmitted by the reader antenna using the technique of wireless power transfer. If the impedance between the tag antenna and chip matches, and the polarization between transmitting and receiving antennas matches, the tag received power can be calculated by

$$P = A_e S_{av}. \tag{1}$$

where $A_e = \frac{\lambda^2}{4\pi} G$, $S_{av} = |\mathbf{E}_{tag}|^2 / 2\eta_0$, and A_e is the effective cross-section of tag antenna, S_{av} is the energy flux density at the tag, η_0 is the free space impedance (377Ω), λ is the wavelength and G is the antenna gain. With X representing polarization matching coefficient between the tag and reader antennas, τ representing matching factor between the chip and the tag antenna, and L_{ws} representing the windscreen penetration loss, the tag received power can be expressed as

$$P = \frac{\lambda^2 G |\mathbf{E}_{tag}|^2 X \tau}{8\pi\eta_0 L_{ws}}. \tag{2}$$

In equation (2), it is critical to calculate the electric field strength $\mathbf{E}_{tag}$ at the position of tag. For an AVI/ETC system, the LOS always exists, and it has minimum propagation delay. Since the time difference among other delays may be small, only several significant delay components can be divided [7]. As Fig. 1 shows, the dominant waves received by the tag are the LOS wave and the waves reflected by the hood and the bus body. These waves play a decisive role on the electric field strength, with the Direction of Arrival (DoA) expressed as $(\theta_m, \phi_m), m = 0, 1, 2$. So the field strength can be expressed as

$$\mathbf{E}_{tag} = \sum_{m=0}^{2} \mathbf{E}_m(\theta_m, \phi_m). \tag{3}$$

where $m = 0, 1, 2$ represent respectively LOS, the hood reflection and the bus body reflection.

In the direction of azimuth (θ, ϕ), y meters away from the reader antenna, the LOS electric field strength can be expressed as

$$E(y, \theta, \phi) = \left(A_\theta(\theta, \phi)\hat{e}_\theta + A_\phi(\theta, \phi)\hat{e}_\phi\right) \frac{e^{-j\beta y}}{y}. \tag{4}$$

with

$$\begin{aligned} A_\theta(\theta, \phi) &= \sqrt{\frac{P_T \eta_0}{2\pi}} g_\theta(\theta, \phi), \\ A_\phi(\theta, \phi) &= \sqrt{\frac{P_T \eta_0}{2\pi}} g_\phi(\theta, \phi), \\ g_\theta(\theta, \phi) &= \sqrt{|G_\theta(\theta, \phi)|} e^{j\psi_\theta}, \\ g_\phi(\theta, \phi) &= \sqrt{|G_\phi(\theta, \phi)|} e^{j\psi_\phi}, \\ \beta &= \frac{\omega}{c}. \end{aligned} \tag{5}$$

where P_T is the reader transmitted power, $\hat{e}_\theta$ and $\hat{e}_\phi$ are the unit vector of the spherical coordinates, $G_\theta(\theta, \phi)$ and $G_\phi(\theta, \phi)$ are the transmitting antenna gain in the direction of $\hat{e}_\theta$ and $\hat{e}_\phi$, ψ_θ and ψ_ϕ are the relative phase of electric field in the distance of y, and direction of $\hat{e}_\theta$ and $\hat{e}_\phi$, β is the wave number, ω is the carrier angular frequency.

In this paper, we use a right-handed circular polarization microstrip antenna as the reader antenna, and its gain can be calculated using

$$\begin{aligned} &G_\theta(\theta, \phi) = G_\phi(\theta, \phi) = \tfrac{3.136}{\sqrt{2}} \cdot \\ &\left(sin(\theta) \tfrac{sin\left(\frac{\pi}{2} cos(\theta)\right)}{cos(\theta)} cos\left(\tfrac{\pi}{2} sin(\theta) sin(\phi)\right) \right)^2 \end{aligned} \tag{6}$$

C. Calculation of Geometric Relations

Commercial ray-tracing software, such as Wireless Insite, is suitable to calculate the multiple reflected RF waves. But people need to build a three-dimensional geometric computer model of the scene and determine the material properties for reflective objects firstly. In the view that the RF strength is mainly determined by the LOS and one time reflected waves in AVI/ETC application scenarios, the geometric relationships can be easily computed through the mirror method [1], [2], [7], [8]. The paper will simulate a typical case that a car needs to be identified with a large vehicle (a bus) inside the adjacent lane, as illustrated in Fig. 1(b).

III. Impact of Vehicle Speed

A. Available Inventory Distance

When the vehicle across the radiation zone A along a specific route with a variable speed, it will experience two states repeatedly. One is the power-up state of tag chip, the other is the power-off state. The direction of main lobe of tag antenna is also changed during moving.

Generally, there are two types of vehicle driving speed in AVI/ETC applications. One is the vehicle constant speed of ETC free flow record or AVI scenarios. The other is the decelerated speed for toll collection scenario. As shown in Fig. 2, a tagged vehicle with a maximum initial speed v_{max} arrives at the ground sensor coil, then it decelerates with an instantaneous speed v. After the data exchange is finished and the barrier is opened, the vehicle, with a minimum speed v_{min}, will accelerate and run away. In most cases, the vehicle will decelerate linearly from v_{max} to v_{min} with an acceleration parameter a, as illustrated in the Figure.

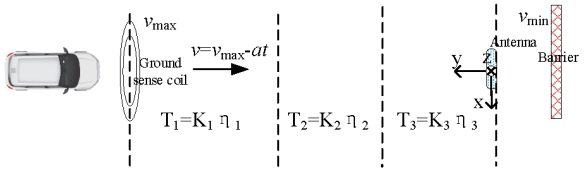

Fig. 2. A schematic of the communication procedure.

In the following, we suppose the tag moves straight in the opposite direction of y-axis, parallel to the xy-plane, and passes through the radiation zone from an initial position. At the moment, the distance to the reader antenna is D_{max}. The total available inventory distance Δ, where the tag will be activated, can be expressed as

$$\Delta = \int_0^{D_{\max}} 1\{P_r(y) \geq P_{th}\} dy \tag{7}$$

where $1\{\cdot\}$ is the indicator function, $P_r(y)$ is the tag received power at position y.

B. Three Processes of Data Exchange

Both the inventory frequency and radiation zone are important to the available total reading times and maximum vehicle speed. So we will analyse this procedure comprehensively. When the tagged vehicle passes through the ETC/AVI zone, mainly three processes for data exchange need to be done. First, when the vehicle reaches the ground sensor coil, the reader will send the inventory QUERY command immediately. At this time, if the tag is activated, the command will be decoded successfully and the random code, RN16, will be returned. The reader will then send the READ command, and the tag will immediately return the ID. Second, the reader will have data access with a remote database after the ID is obtained, including identity verification, fee deduction, and other operations. Third, the reader finally will write data to the tag and open the lane gate at the same time. The tag will also return an ACK signal, as shown in Fig.3(a).

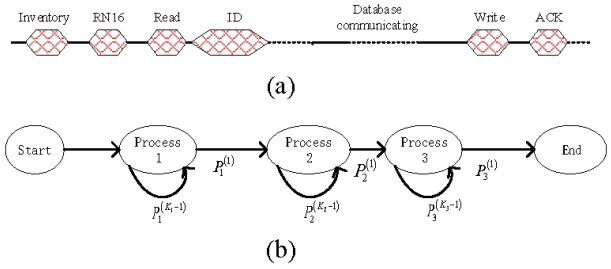

Fig. 3. Three processes and corresponding probability models. (a) Commands & data. (b) Average transition probability among the three processes. Note that the transition between two process will happen with a probability of $P_i^{(1)}$ after $K_i - 1$ times unsuccessful inventory.

Processes 1 and 3 use the air interface to communicate with a Tag. Due to random multipath propagation and interference of other RF emitters, bits error will occur and retransmission will be needed. As shown in Fig.3(b), K_i times retransmission is assumed to be needed with a reader inventory frequency η_i, where $i = 1, 3$. For process 2, the remote database performs data access services at a certain frequency η_2. So the reader may need the time of $K_2 * \eta_2$ to complete the data exchange, where K_2 is the number of services the reader waits. Note that K_i is the average retransmission times.

So the total interactive time T is the sum of the individual used time of the three processes T_i. That is

$$T = \sum_{i=1}^{3} T_i \tag{8}$$

and

$$T_i = \eta_i \cdot K_i \tag{9}$$

where K_i is a random variable, and its sample space is all positive integers.

C. Probability models of the Retransmission & Services Times

The probability of symbol error is determined by the SNR (signal-to-noise ratio), which is the same as the tag received power obtained through the wireless power transfer at a certain noise power. According to the existing research results [11], the probability of successful communication is determined mainly by cascaded channels and is modeled using a sophisticated model. Too many factors have impacts on it. Therefore, we approximately model the probability of successful communication in process $i, i = 1, 3$, as a negative exponential function of tag received power for simplicity. So

$$p_i(\delta_{pow}) = (1 - p_0) e^{-\beta \delta_{pow}} + p_0 \tag{10}$$

where $\delta_{Pow} = P_r(y) - P_{th}$, and p_0 is the probability of the successful communication when $P_r = P_{th}$, and p_0 is assumed to be a constant value in this paper. And $P_r(y)$ is calculated using the prediction method described in Section II. The probability of successful communication after K_i times inventory is expressed as $p_i^{(K_i)}, i = 1, 3$, which is a conditional

probability, as the previous $k_i - 1$ inventory is unsuccessful and the K_ith inventory is successful. So

$$p_i^{(\mathrm{K}_i)} = p\left(\delta_{pow}^{(K_i)}\right) \prod_{k=1}^{K_i-1} \left(1 - p_i^{(k)}\right) \tag{11}$$

where $\delta_{pow}^{(k)} = P_r^{(k)}(y) - P_{th}$. And $P_r^{(k)}(y)$ is the power value at the specific position for the kth inventory, and the distance y to the reader antenna is determined by the tag speed v. So

$$y = D_{\max} - \int_0^{k/\eta_i} v dt \tag{12}$$

For process 2, the communication between the reader and the remote database is usually through a wired channel and surely exists a channel occupying or queuing buffer, so the Poisson distribution can be used to model it. Every communication with the remote database needs to wait for the completion of the previous service. The probability of waiting for K_2 services can be expressed as

$$P_2^{(K_2)} = \sum_{k=1}^{K_2} \frac{\gamma^k e^{-\gamma}}{k!} \tag{13}$$

where γ is the average times of services, it is related to the vehicle speed and frequency of services η_2.

Based on the above analysis, the maximum vehicle speed, and the shortest time to pass through the toll gate can be estimated numerically.

IV. Numerical Results

Based on the equations described in the above two sections, numerical simulations are conducted. The tag received power is calculated followed equations (1) to (5), and three rays are considered with their geometric relations calculated for the scenario in Fig.1. The antenna radiation pattern is calculated from the equation (6). The impacts of tag speed and inventory distance on the inventory performance are simulated based on equation (8)-(12). Table I illustrates the detailed simulation parameters, according to ISO 18000-6C.

Fig. 4 shows the received power distribution for several inclination angles α of reader antenna, using the method in section II. It illustrates how the geometric parameters impact the RF radiation zones. In the simulation, the tag is attached to the windscreen with its height 1.5 meters to the ground. The results show that due to the RF multipath propagation, the received power fluctuates but decreases in the overall tread. When the tag is far away from the reader antenna (in the range from $y = 8$ to $y = 15$), the received power fluctuates around the threshold (for the cases of $\alpha = 15^0$ and 30^0) or a blind area (for the cases of $\alpha = 45^0$ and 60^0). Even close to the reader antenna (at $y = 2$ meters), there is a small number of blind spots (for the case of $\alpha = 15^0$). Due to the polarization mismatching, the received power under the reader antenna (at $y = 0$ meter) is small, which is not enough to activate the tag. The received power on the lane is not symmetrical due to the strong reflection from the large adjacent vehicle on the right side. We also find that the available inventory distance Δ has a close relationship with geometric parameters when deployed. It varies among several meters to 10 meters along the y-axis.

TABLE I
Simulation Parameters

parameters	value
carrier frequency f	915 MHz
e.i.r.p	33 dBm
polarization	circular
tag antenna gain G	2.15 dB
activation sensitivity of passive tag P_{th}	-11 dBm
Polarization matching coefficient X	3 dB
power transmission coefficient τ	0.92
path loss of windscreen L_{WS}	2 dB
height of reader antenna H_{reader}	5 m
height of car hood H_{car}	1 m
height of tag H_{tag}	1.5 m
inclination angle of reader antenna α	15^0,30^0,45^0,60^0
distiance to the bus body D_r	0.7 m
maximum distance D_{max}	10 m
inventory frequency $\eta_i, i = 1, 2, 3$	100 Hz

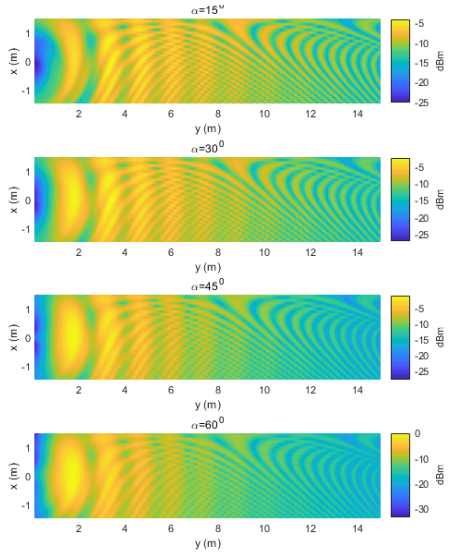

Fig. 4. Tag received power at different inclination angles of reader antenna.

Fig. 5 shows the identification zone corresponding to Fig. 4. In the figure, the white area represents the area where the power received by the tag is greater than the activation threshold of -11 dBm. When the tag moves across the identification zone, the tag will power up and power down repeatedly in the far zone and power down occasionally in the near zone because of the existence of blind spots. The overall available inventory distance Δ will be also different according to equation 7.

Fig. 6 shows the variation of available inventory distance Δ due to different inclination angles α of reader antenna and different activation threshold P_{th}. The results show that the

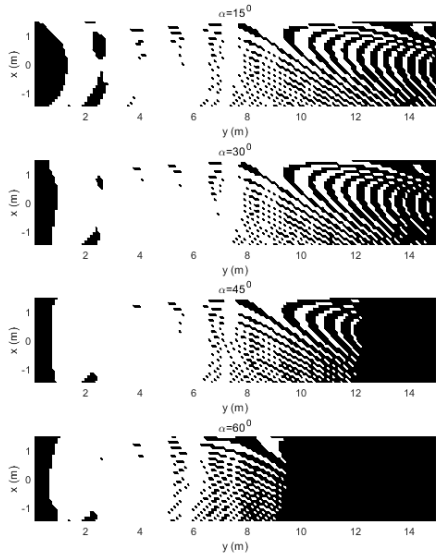

Fig. 5. Corresponding identification zone (white) at different inclination angles of reader antenna for tag threshold $P_{th} = -11$ dBm.

maximum Δ is obtained when $\alpha = 20^0$. We can also increase Δ significantly by improving the sensitivity of the tag chip.

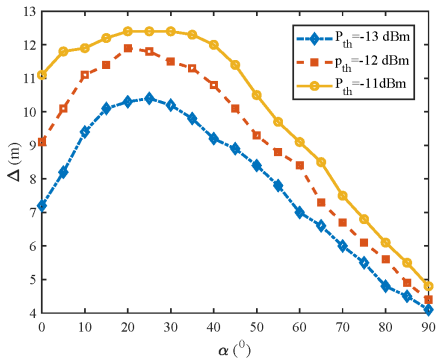

Fig. 6. The impact of inclination angle α of reader antenna to Δ

The impacts of tag speed and available inventory distance Δ on the probability of identification failure are showed in Fig. 7 and Fig. 8. The results illustrate that both factors have serious influences on the failure probability. And for a specific failure probability 0.1, the vehicle speed is very different ($>$ 10 dB) when $\Delta = 12$ meters and $\Delta = 1$ meter. Fig. 8 illustrates that the vehicle speed is more important when $\Delta >= 4$ meters. So we should maximize the Δ to achieve a higher vehicle speed by optimizing geometric parameters. On the other hand, it also needs to control the vehicle speed to obtain an ideal identification rate for a specific available inventory distance.

V. Conclusion

The paper focuses on the performance of RFID based AVI/ETC systems. The influences of RF radiation zone and vehicle speed were considered. The RF radiation zone was

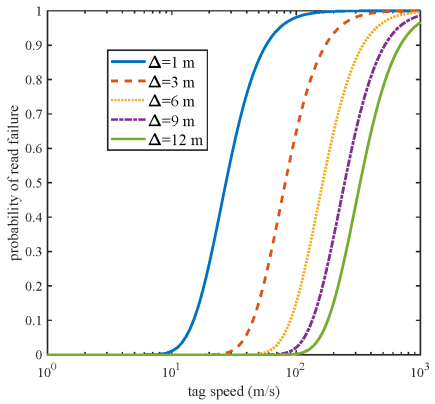

Fig. 7. The impact of tag speed

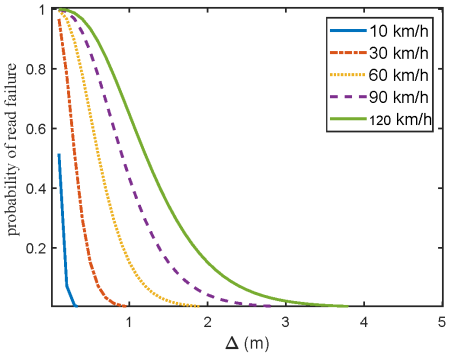

Fig. 8. The impact of available inventory distance Δ

related to the geometric parameters for a typical scene through a multi-ray method. So, a more accurate identification zone can be calculated compared to the statistical method. After dividing the whole communication procedure into three processes, suitable probability distributions were used to model the impact of vehicle speed and the available inventory distance simultaneously. We found that the geometric parameters are very important to achieve a wider identification zone and higher vehicle passing speed. We can optimize them more exactly based on the proposed method. Future research on this topic could include the performance of passive RFID AVI/ETC systems under high-speed multi-tag conditions.

References

[1] B. Li, Q. Huan, L. Zuo, B. Yin, F. Guo, and Y. He, Impact of Vehicle Head Geometric Features in the Propagation Loss of ETC System, IEEE Intell. Transp. Syst. Mag., vol. 9, no. 3, pp. 88-99, 2017.

[2] C. Pedraza, F. Vega, and G. Manana, PCIV, an RFID-Based Platform for Intelligent Vehicle Monitoring, IEEE Intell. Transp. Syst. Mag., vol. 10, no. 2, pp. 28-35, 2018.

[3] J. D. Griffin and G. D. Durgin, Complete Link Budgets for Backscatter-Radio and RFID Systems, IEEE Antennas Propag. Mag., vol. 51, no. 2, pp. 11-25, Apr. 2009.

[4] G. Marrocco, E. Di Giampaolo, and R. Aliberti, Estimation of UHF RFID Reading Regions in Real Environments, IEEE Antennas Propag. Mag., vol. 51, no. 6, pp. 44-57, Dec. 2009.

[5] M. Abbak and I. Tekin, RFID Coverage Extension Using Microstrip-patch Antenna Array [Wireless Corner], IEEE Antennas Propag. Mag., vol. 51, no. 1, pp. 185-191, 2009.
[6] D. Inserra, W. Hu, and G. Wen, Antenna Array Synthesis for RFID-Based Electronic Toll Collection, IEEE Trans. Antennas Propag., vol. 66, no. 9, pp. 4596-4605, Sep. 2018.
[7] L. Azpilicueta, C. Vargas-Rosales, and F. Falcone, Intelligent Vehicle Communication: Deterministic Propagation Prediction in Transportation Systems, IEEE Veh. Technol. Mag., vol. 11, no. 3, pp. 29-37, Sep. 2016.
[8] A. L. Xavier, S. Celaschi, N. T. Azana, P. Shieh, and T. E. de A. Santos, Radio-Frequency Identification Zones in Open Environments: Maximizing the Reading Probability of High-speed tags, IEEE Antennas Propag. Mag., vol. 59, no. 4, pp. 62-72, Aug. 2017.
[9] A. A. Larionov, R. E. Ivanov, and V. M. Vishnevsky, UHF RFID in Automatic Vehicle Identification: Analysis and Simulation, IEEE J. Radio Freq. Identif., vol. 1, no. 1, pp. 312, 2017.
[10] K. Haneda, J. I. Takada, T. Iwata, Y. Wakinaka, and T. Kunishima, Experimental determination of propagation paths for the ETC system - Equipment development and field test, IEICE Trans. Fundam. Electron. Commun. Comput. Sci., vol. E87-A, no. 11, pp. 30083015, 2004.
[11] A. Bekkali, S. Zou, A. Kadri, M. Crisp, and R. Penty, Performance Analysis of Passive UHF RFID Systems Under Cascaded Fading Channels and Interference Effects, IEEE Trans. Wirel. Commun., vol. 14, no. 3, pp. 14211433, Mar. 2015.